# Sequential Nature of $(p,3p)$ Two-Proton Knockout from Neutron-Rich Nuclei

A. Frotscher,[1,*] M. Gómez-Ramos,[1] A. Obertelli,[1,2,3] P. Doornenbal,[3] G. Authelet,[2] H. Baba,[3] D. Calvet,[2] F. Château,[2] S. Chen,[4,3] A. Corsi,[2] A. Delbart,[2] J.-M. Gheller,[2] A. Giganon,[2] A. Gillibert,[2] T. Isobe,[3] V. Lapoux,[2] M. Matsushita,[5] S. Momiyama,[3,6] T. Motobayashi,[3] M. Niikura,[6] H. Otsu,[3] N. Paul,[2,3] C. Péron,[2] A. Peyaud,[2] E. C. Pollacco,[2] J.-Y. Roussé,[2] H. Sakurai,[3,6] C. Santamaria,[2,3] M. Sasano,[3] Y. Shiga,[7] N. Shimizu,[8] D. Steppenbeck,[3] S. Takeuchi,[3] R. Taniuchi,[3,6] T. Uesaka,[3] H. Wang,[3] K. Yoneda,[3] T. Ando,[3,6] T. Arici,[9,10] A. Blazhev,[11] F. Browne,[12] A. M. Bruce,[12] R. Carroll,[13] L. X. Chung,[14] M. L. Cortés,[1,9,3] M. Dewald,[11] B. Ding,[15] Zs. Dombradi,[16] F. Flavigny,[17,†] S. Franchoo,[17] F. Giacoppo,[18,9] M. Górska,[9] A. Gottardo,[17] K. Hadyńska-Klęk,[18] Z. Korkulu,[16] S. Koyama,[3,6] Y. Kubota,[1,3,5] A. Jungclaus,[19] J. Lee,[20] M. Lettmann,[1] B. D. Linh,[14] J. Liu,[20] Z. Liu,[15,21] C. Lizarazo,[9,1] C. Louchart,[1] R. Lozeva,[22,23] K. Matsui,[3,6] T. Miyazaki,[3,6] K. Moschner,[11] S. Nagamine,[6,3] N. Nakatsuka,[24] C. Nita,[25] S. Nishimura,[3] C. R. Nobs,[12] L. Olivier,[17] S. Ota,[5] Z. Patel,[13] Zs. Podolyák,[13] M. Rudigier,[13] E. Sahin,[18] T. Y. Saito,[6,3] C. Shand,[13] P.-A. Söderström,[3,26] I. G. Stefan,[17] T. Sumikama,[27] D. Suzuki,[17] R. Orlandi,[28] V. Vaquero,[19] Zs. Vajta,[16] V. Werner,[1] K. Wimmer,[6,3] J. Wu,[3,4] and Z. Xu[20]

[1]*Institut für Kernphysik, Technische Universität Darmstadt, D-64289 Darmstadt, Germany*
[2]*IRFU, CEA, Université Paris-Saclay, F-91191 Gif-sur-Yvette, France*
[3]*RIKEN Nishina Center, 2-1 Hirosawa, Wako, Saitama 351-0198, Japan*
[4]*School of Physics and State Key Laboratory of Nuclear Physics and Technology, Peking University, Beijing 100871, People's Republic of China*
[5]*Center for Nuclear Study, The University of Tokyo, RIKEN campus, Wako, Saitama 351-0198, Japan*
[6]*Department of Physics, The University of Tokyo, 7-3-1 Hongo, Bunkyo, Tokyo 113-0033, Japan*
[7]*Department of Physics, Rikkyo University, 3-34-1 Nishi-Ikebukuro, Toshima, Tokyo 172-8501, Japan*
[8]*Center for Nuclear Study, The University of Tokyo, 7-3-1 Hongo, Bunkyo, Tokyo 113-0033, Japan*
[9]*GSI Helmholtzzentrum für Schwerionenforschung GmbH, D-64291 Darmstadt, Germany*
[10]*Justus-Liebig-Universität Giessen, D-35392 Giessen, Germany*
[11]*Institut für Kernphysik, Universität zu Köln, D-50937 Köln, Germany*
[12]*School of Computing Engineering and Mathematics, University of Brighton, Brighton BN2 4GJ, United Kingdom*
[13]*Department of Physics, University of Surrey, Guildford GU2 7XH, United Kingdom*
[14]*Institute for Nuclear Science & Technology, VINATOM, P.O. Box 5T-160, Nghia Do, Hanoi, Vietnam*
[15]*Institute of Modern Physics, Chinese Academy of Sciences, Lanzhou 730000, People's Republic of China*
[16]*MTA Atomki, P.O. Box 51, Debrecen H-4001, Hungary*
[17]*Present affiliation: LPC Caen, ENSICAEN, Université de Caen, CNRS/IN2P3, 14050 Caen Cedex 04, France*
[18]*Department of Physics, University of Oslo, N-0316 Oslo, Norway*
[19]*Instituto de Estructura de la Materia, CSIC, 28006 Madrid, Spain*
[20]*Department of Physics, The University of Hong Kong, Pokfulam, Hong Kong*
[21]*School of Nuclear Science and Technology, University of Chinese Academy of Sciences, Beijing 100049, China*
[22]*IPHC, CNRS/IN2P3, Université de Strasbourg, F-67037 Strasbourg, France*
[23]*CSNSM, CNRS/IN2P3, Université Paris-Sud, F-91405 Orsay Campus, France*
[24]*Department of Physics, Faculty of Science, Kyoto University, Kyoto 606-8502, Japan*
[25]*Horia Hulubei National Institute of Physics and Nuclear Engineering (IFIN-HH), RO-077125 Bucharest, Romania*
[26]*Extreme Light Infrastructure-Nuclear Physics (ELI-NP), 077125 Bucharest-Măgurele, Romania*
[27]*Department of Physics, Tohoku University, Sendai 980-8578, Japan*
[28]*Advanced Science Research Center, Japan Atomic Energy Agency, Tokai, Ibaraki 319-1195, Japan*

(Received 6 December 2019; revised 27 February 2020; accepted 1 June 2020; published 30 June 2020)

Twenty-one two-proton knockout $(p,3p)$ cross sections were measured from neutron-rich nuclei at ~250 MeV/nucleon in inverse kinematics. The angular distribution of the three emitted protons was determined for the first time, demonstrating that the $(p,3p)$ kinematics are consistent with two sequential proton-proton collisions within the projectile nucleus. Ratios of $(p,3p)$ over $(p,2p)$ inclusive cross sections follow the trend of other many-nucleon removal reactions, further reinforcing the sequential nature of $(p,3p)$ in neutron-rich nuclei.

DOI: 10.1103/PhysRevLett.125.012501

*Introduction.*—The nuclear shell model has been remarkably successful in describing the overall properties of atomic nuclei [1–3], but the structural evolution as a function of proton-to-neutron asymmetry remains an outstanding questions in quantum physics [4]. This shell evolution originates in the properties of the many-body nuclear interactions and is currently the focus of intense study, motivating the development of dedicated new generation radioactive beam facilities [5–9] and new experimental methods. In particular, one-nucleon knockout reactions at intermediate energies, above ∼50 MeV/nucleon, have been extensively used for the spectroscopy of unstable isotopes, both with heavy-ion [10,11] and proton targets [12,13]. Given the success of one-nucleon knockout reactions, two-nucleon knockout has naturally garnered much interest, as it allows us to explore further nuclear properties, such as nucleon-nucleon correlations [14–18]. Two-proton knockout from neutron-rich nuclei has been used to populate very exotic species, in a process assumed to be direct, due to the inhibited proton evaporation in these nuclei [19–23]. In particular, two-proton knockout on a proton target, $(p,3p)$, is a promising probe. The reaction $^{80}$Zn$(p,3p)$ has recently been used to populate new $^{78}$Ni states, inaccessible to one-nucleon knockout [24], demonstrating the potential of $(p,3p)$ reactions as a spectroscopic tool for exotic nuclei. However, to properly interpret the resulting observables, the $(p,3p)$ reaction mechanism must be well understood, as the removal of spatially correlated proton pairs [18] explores different nuclear properties than the sequential removal of uncorrelated protons [15,25]. For example, the residual nucleus momentum distribution explores its nuclear structure when removing uncorrelated protons [19], while removing a short-range correlated proton pair makes it sensitive to the pair momentum distribution, which is weakly $A$ dependent [26].

In this Letter we demonstrate that $(p,3p)$ from neutron-rich nuclei at intermediate energies takes place mainly through two sequential proton-proton collisions. We analyzed 21 $(p,3p)$ reactions (mass numbers 68 to 112, mean neutron-to-proton ratio 1.6 [27]), using a unique setup [28] to measure the angular distributions of the three emitted protons event by event. Inclusive cross sections were also measured.

*Experiment.*—The measurements were conducted at the Radioactive Isotope Beam Factory (RIBF), operated by the RIKEN Nishina Center and the Center for Nuclear Study of the University of Tokyo. They were divided into two consecutive experimental campaigns, containing three and four settings each. A $^{238}$U beam was accelerated to 345 MeV/nucleon and impinged onto a 3 mm beryllium target. The average beam intensity was 12 pnA for the first campaign and 30 pnA for the second.

Radioactive beams were produced via in-flight abrasion-induced fission [29] and were identified with the so-called

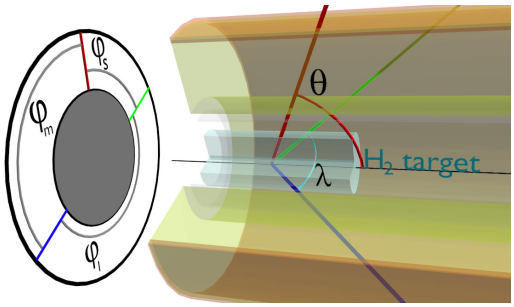


FIG. 1. Overview of the secondary target area. The liquid hydrogen target (blue) is surrounded by the MINOS time projection chamber (yellow), which tracked the scattered protons. The angle between each proton and the beam axis $\theta$, the angle between each pair of protons $\lambda$ and the angles between the protons in the plane perpendicular to the beam axis $\varphi_s \leq \varphi_m \leq \varphi_l$ are drawn.

$B\rho-\Delta E-$TOF method through the BigRIPS spectrometer [30]. The magnetic rigidity ($B\rho$), energy loss ($\Delta E$) and time of flight (TOF) were obtained by parallel plate avalanche counters [30], ionization chamber and plastic scintillators, respectively. These beam particles impinged with an energy of ∼250 MeV/nucleon onto the liquid hydrogen ($LH_2$) target of 102(1) and 99(1) mm thickness for the first and second campaign, respectively [28]. The $LH_2$ target was contained with 110 $\mu$m entrance and 150 $\mu$m exit Mylar windows. Emitted protons were detected using MINOS [28], a vertex tracker consisting of a time projection chamber (TPC) surrounding the target as shown in Fig. 1. A full reconstruction of the track was performed through a Hough transformation [31–33], yielding the three-dimensional vertex position and the angles between the protons and the beam. The combined angular resolution for individual tracks was ∼7° (FWHM) while the efficiency for the detection of three tracks in a $(p,3p)$ event was ∼21% [51% for two tracks in a $(p,2p)$ event]. Reaction channels were identified via the detected fragments. The energy of the outgoing protons was not measured. After typical energy loss of 70–100 MeV/nucleon in the target, the unreacted beam particles and fragments were identified via $B\rho-\Delta E-$TOF and separated by the ZeroDegree spectrometer (ZDS) [34], operated in the large momentum acceptance mode ±3%. Thus, only bound final states were measured. Details of the experimental campaigns can be found in [24,35–42]. Events considered for the cross section determination were triggered by a thin plastic scintillator few meters upstream the hydrogen target. The acquisition was operated in a common-dead-time mode. The acquisition rate ranged typically from 100 to 600 Hz. The inclusive $(p,3p)$ and $(p,2p)$ cross sections $\sigma$ were evaluated with:

$$\sigma = \frac{1}{n_{H_2}\tau}\frac{N_o}{N_i}\left(\frac{1}{1+\nu}\right) \quad (1)$$

with the number of identified particles in BigRIPS and ZDS, $N_i$ and $N_o$, which were selected in momentum to pass through ZDS. $n_{H_2}$ was the areal density of the liquid hydrogen target, $\tau$ the transmission from the beam trigger detector at the end of BigRIPS to the end of ZDS and $\nu$ the areal density ratio between the material downstream the $LH_2$ target and the $LH_2$ target itself. $\tau$, combining both the ZDS transmission and the ZDS detector efficiency [93(4)% from empty target runs], ranged from 47(6)% to 60(6)%. $\nu$ was 4.8%(4.4%) for the first (second) campaign. Dead-time effects cancel in Eq. (1). The target density was calculated from the density of the $LH_2$, and determined to be 70.97(3) g/l for the first campaign, and 73.22(8) g/l for the second, $n_{H_2}$ was 4.32(4) and $4.33(4) \times 10^{23}$ atoms/cm$^2$, respectively [35]. Only fully stripped ions identified in ZDS were considered. For $(p,3p)$, the number of events where two consecutive $(p,2p)$ reactions take place inside the target have been estimated [from 2(1) to 17(2)% for the studied cases and 5(1)% for $^{81}$Ga$(p,3p)$ discussed below] and subtracted. The particle identification of $(p,3p)$ fragments in ZDS can be contaminated by hydrogen-like fragments ($q = Z - 1$), after two-proton and several-neutron removal, if their mass-over-charge ratio is close enough to the fragment of interest. Although the proportion of hydrogen-like ions is of the level of few percents compared to the fully stripped ions, the channels contribute from 0.3(1)% to 47(14)% [6(2)% for $^{81}$Ga] to the $(p,3p)$ particle identification within the $A/q$ resolution of ZDS. The information from the TPC was not used for the extraction of the inclusive cross sections. Experimental uncertainties [27] were dominated by statistics of the fragments and the charge state subtraction.

As the reaction products were shifted partly out of momentum acceptance in ZDS, the transmission was determined through simulations with LISE$_{++}$ [43]. They comprised the second half of the BigRIPS spectrometer, the $LH_2$ target and the ZDS. Simulations include momentum acceptance, $(p,xp)$ reactions in the target and reactions with material in the beam line. $B\rho$ settings and materials in the beam were verified using the experimental transmission obtained from $(p,2p)$ reactions of the same setting. The beam profile and momentum distribution used as input to the simulations were fitted to experimental data. The transmission $\tau$ ranged from 47(6)% ($Z = 42$) to 60(6)% ($Z = 27$), including the ZDS detection efficiency [93(4)%]. Uncertainties were extracted from dedicated transmission runs, where ZDS was tuned to let the unreacted beam pass. The upper (lower) acceptance cuts in momentum were selected such that at least 96% (99%) of the reacted beam traversed ZDS. The corresponding upper (lower) cuts in magnetic rigidity ranged from 6.72(6.48) to 7.08(6.82) Tm.

*Results and discussion.*—The measured inclusive cross sections are displayed on the left panel of Fig. 2 and tabulated in [27]. The $(p,3p)$ cross sections are smaller than $(p,2p)$ by about $10^{-2}$. They range from 0.014(9) mb [$^{101}$Sr$(p,3p)$] to 0.37(6)mb [$^{75}$Zn$(p,3p)$]. Systematics of the $(p,2p)$ reaction based on the same experimental data are published in [35]. On the right side of Fig. 2, the ratio of $(k+1)$-nucleon-removal to $k$-nucleon-removal cross sections, considering only nucleons of the same species, is plotted over the evaporation cost asymmetry $\Delta C$, as in [44]. $\Delta C$ is a measure for the imbalance between evaporating a proton (neutron) versus evaporating a neutron (proton) in proton (neutron) removal reactions. It is calculated for each daughter nucleus of the $k$-nucleon removal reaction: $\Delta C = \mp S_n \pm (S_p + V_C)$, for proton (upper signs) and neutron (lower signs) removal with $S_{p(n)}$ being the proton (neutron) separation energy and $V_C$ the Coulomb barrier [45]. The general trend in [44] is followed by the present ratios. This trend for proton-deficient nuclei ($\Delta C > 0$) has been understood as uncorrelated multiple nucleon removals. Thus, the $(p,3p)$ reaction is likely to be of sequential nature. To further constrain our understanding of the reaction mechanism, we compare angular distributions of the emitted protons to three kinematical models:

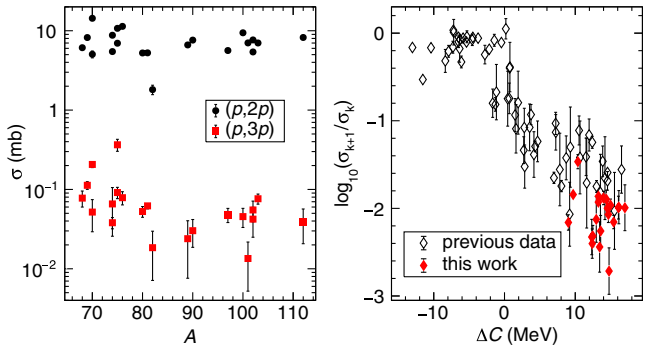


FIG. 2. (Left) Experimental $(p,2p)$ and $(p,3p)$ cross sections [27]. Error bars contain systematic and statistic uncertainties added in quadrature. (Right) Ratio $(\sigma_{k+1}/\sigma_k)$ of $(k+1)$-nucleon and $k$-nucleon removal cross sections with removed nucleons from same species (open markers) as a function of the evaporation cost asymmetry $\Delta C$, with $k = 1$–9. The data are taken from [44,50–56]. See [44] for details. Ratios of $(p,3p)$ over $(p,2p)$ cross sections for the same incident nucleus from this Letter are shown (red diamonds).

(i) Sequential: The nucleus interacts with one target proton. Two consecutive proton-proton collisions happen inside the nucleus, each collision following the free proton-proton cross section. Isotropic emission of the colliding protons in their center of mass is assumed. Test calculations with anisotropic proton-proton cross sections from [46] show the same features. The cross section energy dependence is taken from [47]. Apart from the projectile momentum, the protons inside the nucleus are assumed to have an intrinsic momentum following a Gaussian distribution, with rms momentum $\sqrt{\langle p^2 \rangle} = p_{\mathrm{nuc}}$. The $(p,2p)$ reaction was modelled in a similar way, considering just one collision.

(ii) Pair breakup: The two removed protons are assumed to form a correlated pair, with each proton having a momentum $p_{\mathrm{nuc}}$, and the overall pair having zero total momentum in the projectile rest frame. Pair orientation is assumed to be isotropic. During the collision, the target proton interacts with only one of the protons of the pair, following the free proton-proton cross section. The other proton of the pair acts as a spectator and is emitted with its original momentum. This process is similar to the impulse approximation usually assumed in high-energy $(e, e'2p)$ and $(p, 3p)$ reactions [18,26,48].

(iii) Pair knockout: The two removed protons are assumed to be in a correlated pair, as in the pair breakup model. During the collision, the target proton interacts with the whole pair as with a deuteron, following the elastic $p, d$ angular distribution, taken from [49]. Afterwards, the protons in the pair are each emitted with their intrinsic momentum plus half the pair momentum after the collision.

All models consider the interaction between the protons and the residual nucleus assuming that if one of the protons has an energy lower than a given $E_{\mathrm{thresh}}$ in the projectile rest frame it will be absorbed. Furthermore, we model the deflection of the outgoing protons by the residual nucleus by adding a random momentum to each of the protons, taken from a Gaussian distribution with a width of $p_{\mathrm{def}}$, and a mean of $(0, 0, +p_{\mathrm{def}})^{\intercal}$ in the direction of the beam to reflect the pull of the residual nucleus over the proton.

The chosen angular observables are $\theta$, the angle between the outgoing protons and the beam, $\lambda$, the relative angle between each pair of protons, and $\varphi_s$ and $\varphi_m$, the smallest and second smallest angles that each pair of protons form in the plane perpendicular to the beam. For $(p, 3p)$, $\varphi_l$, the largest angle, fulfills $\varphi_s + \varphi_m + \varphi_l = 360°$. An illustration of these observables is given in Fig. 1. Note that each $(p, 2p)$ event contributes one $\lambda$ and two $\theta$ while each $(p, 3p)$ contributes three $\lambda$ and three $\theta$.

The three parameters $p_{\mathrm{nuc}} = 200$ MeV/c, $E_{\mathrm{thresh}} = 30$ MeV and $p_{\mathrm{def}} = 18$ MeV/c have been adjusted to reproduce experimental relative $\lambda$ and beam $\theta$ angle distributions for the two outgoing protons in $^{81}$Ga$(p, 2p)$, assuming a quasifree model. The values for $p_{\mathrm{nuc}}$ and $E_{\mathrm{thresh}}$ are close to the standard values for Fermi momentum and potential well in the INCL model: 270 MeV/c and 40 MeV, respectively [57]. Events generated with each model are then used as an input for GEANT4 simulations [58], to replicate the analysis on experimental data. The chosen observables did not vary significantly depending on the nucleus. Therefore we focused on $^{81}$Ga$(p, 3p)^{79}$Cu and $^{81}$Ga$(p, 2p)^{80}$Zn, for which statistics were the largest. Events exceeding a vertex uncertainty of 10 mm have been omitted. Models were normalized to the experimental number of counts.

In Fig. 3, the double distribution for the $\varphi_s$ and $\varphi_m$ angles is plotted for $^{81}$Ga$(p, 3p)$ and the three models. The phase space is restricted to a triangle, as $\varphi_l \geq \varphi_m \geq \varphi_s$. The

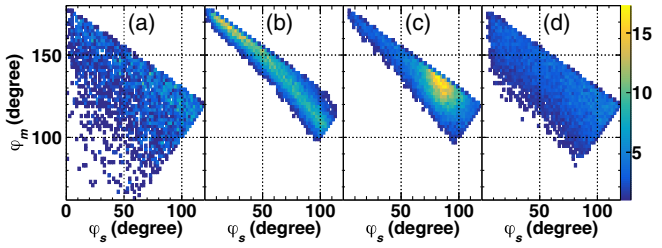


FIG. 3. Two-dimensional plot for a $(p, 3p)$ reaction of the two smaller angles $\varphi_s$ and $\varphi_m$ in the plane perpendicular to the beam axis. (a) Experimental data for $^{81}$Ga$(p, 3p)$ (b) pair breakup model (c) pair knockout model (d) sequential model. Theoretical distributions have been normalized to the data.

experimental data shows that the angular distribution is largely symmetric: $\varphi_m \sim 180° - \varphi_s/2$, but has a wide spread to smaller $\varphi_s$, $\varphi_m$. The sequential model reproduces the features of the experiment remarkably. The pair breakup and pair knockout models do not reproduce the experimental distribution [27]. The comparison between the quasifree model and $(p, 2p)$ data is presented in the insets of Fig. 4, finding a good reproduction of data for all observables. We performed four different fits to $(p, 2p)$ observables: fitting $\lambda$ and $\theta$ separately, letting $p_{\mathrm{def}}$ vary or fixing it to 18 MeV/c for each observable, as it is essential to reproduce the position of the peak of the $(p, 2p)$ $\lambda$ distribution. The envelope of all of these results is shown as the translucent band around the best fit line in Fig. 4, both for $(p, 2p)$ and $(p, 3p)$ reactions. In the main panels of Fig. 4, the distributions for $\varphi_s$ (top), $\theta$ (middle), and $\lambda$ (bottom) are shown for $^{81}$Ga$(p, 3p)$.

For $\varphi_s$ (top panel), the sequential model follows the data closely over the full range. The pair breakup model agrees similarly well, but fails to reproduce the tail above 105°. The pair knockout model does not reproduce the data.

For $\theta$ (middle panel), MINOS acceptance cuts angles below 10°. The sequential model reproduces remarkably the experimental shape, as opposed to the other models. The pair breakup model features a strong peak at 15°, caused by the small intrinsic momentum of the spectator proton, while the pair knockout model shows a sharp peak at ∼30°, which corresponds to the maximum $\theta$ of $d$, $p$ elastic scattering in inverse kinematics.

For $\lambda$, none of the models describes fully experiment, with the sequential model showing the least disagreement, with the peak position shifted by 10°. The pair breakup model produces a markedly different shape, with a prominent peak at 85°, easily understood as the quasifree peak between the two colliding protons. The pair knockout model increases with a larger slope than the data, peaking at 45°, and then drops off for smaller angles than the data.

For the three observables considered, the best agreement has been obtained with the sequential model. As the translucent bands in Fig. 4 show, a variation on the parameters of the kinematical models does not significantly

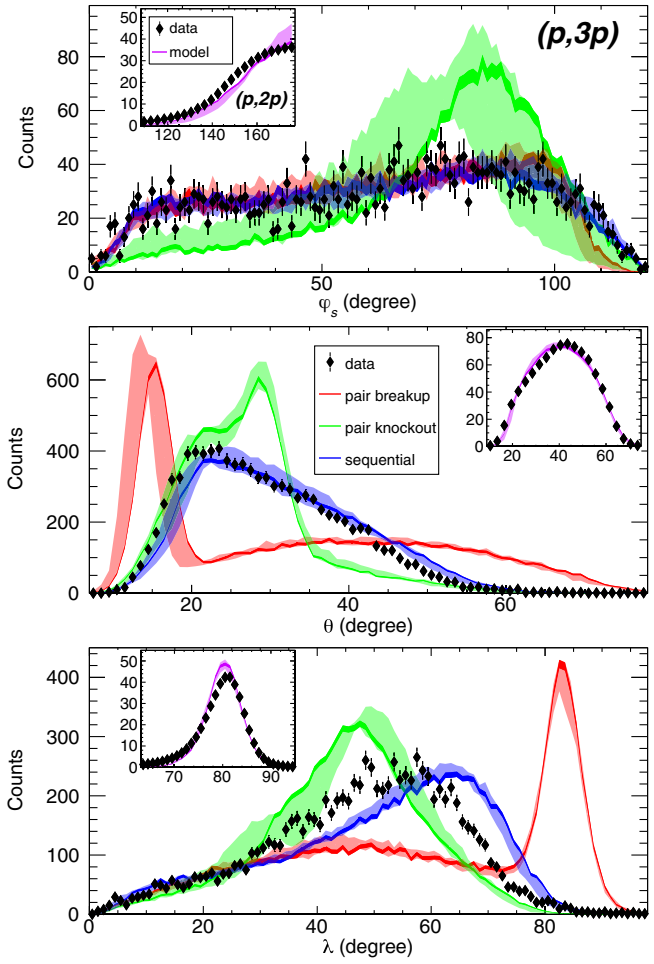


FIG. 4. Distribution for the projected angle $\varphi_s$ (top), the beam angle $\theta$ (middle) and the angle between the scattered protons $\lambda$ (bottom) for $^{81}$Ga$(p,3p)$ and $^{81}$Ga$(p,2p)$ (in insets). Predictions from pair breakup, pair knockout, and sequential model are superposed. Translucent bands show the dependence on the model parameters (see text for details).

modify the features in $(p,3p)$ observables, showing the robustness of these conclusions with respect to the model parameters. A fit of the models in $\varphi_s$ and $\theta$ simultaneously [59] yields contributions of $86^{+10}_{-6}$% for sequential, $14^{+7}_{-10}$% for pair knockout and $0^{+2}_{-0}$% for pair breakup processes with a reduced $\chi^2 = 0.79$, demonstrating the sequential nature of this reaction. Assuming a Gaussian distribution for the pair momentum leads to the same proportions, although somewhat broader distributions [27]. For $^{69}$Co$(p,3p)$ [$^{70}$Ni$(p,3p)$], the sequential contribution is $100^{+0}_{-24}$% ($82^{+18}_{-16}$%) [27]. These results set a solid basis for a quantitative description of the $(p,3p)$ reaction at intermediate energies, opening a new probe for nuclear structure. In particular, this work shows that $(p,3p)$ reactions allow us to populate two-particle-two-hole states in a direct way, and are therefore suitable to study quantitatively and systematically intruder states in neutron-rich nuclei [24], i.e., low-energy correlated states with a dominant multiparticle-multi-hole configuration, as well as shape transitions in a similar way as two-nucleon transfer with stable nuclei [60]. The typical time between the two proton-proton collisions is $10^{-24}$ s, meaning that the wave function of the projectile does not rearrange between collisions, making $(p,3p)$ a candidate for a rescattering probe, currently unexplored in nuclear physics but similar to successful ones in hadronic [61,62] and molecular [63,64] physics. Previous works have shown a relative importance of correlated pairs of around 50% in two-nucleon knockout at lower energies (93 MeV/nucleon) with heavier targets [14]. We have not found such a strong contribution of correlated pairs, possibly due a larger mean free path of the protons in the nucleus.

*Conclusion.*—We have presented 21 new $(p,3p)$ cross sections from neutron-rich medium-mass nuclei at energies of ~250 MeV/nucleon. For the first time, the angular distributions of the three outgoing protons have been measured thanks to the unique combination of the MINOS charged-particle tracker and liquid hydrogen target. These angular distributions were compared to three kinematical models, obtaining for the sequential model a very good agreement, while other models show poor reproduction of the data. These results show that the $(p,3p)$ reaction proceeds via sequential knockout of the protons, which is supported by the ratios $\sigma_{(p,3p)}/\sigma_{(p,2p)}$, following the systematics of [44]. The sequential description of the $(p,3p)$ reaction from neutron-rich nuclei at intermediate energies is therefore a reliable approximation for a quantitative description opening new opportunities, for instance, to explore intruder states and shape transitions towards the neutron dripline.

We thank the RIBF and BigRIPS teams for providing a stable beam and optimum settings over the two experimental campaigns. A. F. acknowledges support from the DFG under Grant No. SFB1245. M. G.-R. acknowledges support from the Alexander von Humboldt foundation. A. O. thanks the European Research Council for its support through ERC Grant No. MINOS-258567, the JSPS Japanese Society for the Promotion of Science for the long-term fellowship L-13520, the German DFG for its support from the SFB Grant No. 1245, and the Alexander von Humboldt Foundation for its support. K. Mo. acknowledges support from German BMBF Grant No. 05P15PKFNA. M. L. C., M. L., and V. W. acknowledge support from German BMBF Grants No. 05P15RDFN1, and No. 05P19RDFN1, as well as DFG Grant No. SFB 1245. L. X. C. and B. D. L. are supported by the Vietnam MOST through Physics Development Program Grant No. Đ TĐ LCN.25/18 and acknowledge the Radioactive Isotope Physics Laboratory of the RIKEN Nishina Center for supporting their stay during the experiment. A. J. and V. V. acknowledge support from the Spanish Ministerio de Economía y

Competitividad under Contract No. FPA2017-84756-C4-2-P. U.K. participants acknowledge support from the Science and Technology Facilities Council (STFC). Collaborators from I. M. P. were supported by the National Natural Science Foundation of China and the Chinese Academy of Sciences. R. T. was supported by the JSPS Grant-in-Aid for JSPS Research Fellows JP14J08718. Zs. D., Z. K., and Zs. V. acknowledge the support from Projects No. OTKA K128947 and No. GINOP-2.3.3-15-2016-00034. C. Santamaria acknowledges support by the IPA program at the RIKEN Nishina Center.

*afrotscher@ikp.tu-darmstadt.de
†Present address: Institut de Physique Nucléaire, CNRS-IN2P3, Université Paris-Sud, Université Paris-Saclay, F-91406 Orsay Cedex, France.

[1] M. G. Mayer, Phys. Rev. **75**, 1969 (1949).
[2] A. Bohr and B. R. Mottelson, Nuclear Structure: Volume I: Single-Particle Motion Volume (World Scientific Publishing Co. Pte. Ltd., Singapore, 1998).
[3] J. French, E. Halbert, J. McGrory, and S. Wong, in *Advances in Nuclear Physics*, edited by M. Baranger and E. Vogt (Springer, Boston, 1969), pp. 193–259.
[4] O. Sorlin and M.-G. Porquet, Prog. Part. Nucl. Phys. **61**, 602 (2008).
[5] H. Okuno, N. Fukunishi, and O. Kamigaito, Prog. Theor. Exp. Phys. **2012**, 03C002 (2012).
[6] P. Spiller and G. Franchetti, Nucl. Instrum. Methods Phys. Res., Sect. A **561**, 305 (2006).
[7] J. Wei *et al.*, in *Proceedings, 26th International Linear Accelerator Conference (LINAC12): Tel Aviv, Israel, 2012* (Curran, Red Hook, 2013), pp. 417–421.
[8] A. Andrighetto *et al.*, Nucl. Phys. **A834**, 754c (2010).
[9] J. Yang *et al.*, Nucl. Instrum. Methods Phys. Res., Sect. B **317**, 263 (2013).
[10] E. Sauvan *et al.*, Phys. Rev. C **69**, 044603 (2004).
[11] P. Hansen and J. Tostevin, Annu. Rev. Nucl. Part. Sci. **53**, 219 (2003).
[12] T. Aumann, C. A. Bertulani, and J. Ryckebusch, Phys. Rev. C **88**, 064610 (2013).
[13] T. Wakasa, K. Ogata, and T. Noro, Prog. Part. Nucl. Phys. **96**, 32 (2017).
[14] K. Wimmer *et al.*, Phys. Rev. Lett. **109**, 202505 (2012).
[15] E. C. Simpson, J. A. Tostevin, D. Bazin, B. A. Brown, and A. Gade, Phys. Rev. Lett. **102**, 132502 (2009).
[16] E. C. Simpson and J. A. Tostevin, Phys. Rev. C **83**, 014605 (2011).
[17] C. Bertulani, Nucl. Phys. **A767**, 155 (2006).
[18] S. Stevens, J. Ryckebusch, W. Cosyn, and A. Waets, Phys. Lett. B **777**, 374 (2018).
[19] D. Bazin, B. A. Brown, C. M. Campbell, J. A. Church, D. C. Dinca, J. Enders, A. Gade, T. Glasmacher, P. G. Hansen, W. F. Mueller, H. Olliver, B. C. Perry, B. M. Sherrill, J. R. Terry, and J. A. Tostevin, Phys. Rev. Lett. **91**, 012501 (2003).
[20] A. Gade *et al.*, Phys. Rev. C **74**, 021302(R) (2006).
[21] P. Adrich *et al.*, Phys. Rev. C **77**, 054306 (2008).
[22] A. Gade *et al.*, Phys. Rev. Lett. **99**, 072502 (2007).
[23] J. Fridmann *et al.*, Nature (London) **435**, 922 (2005).
[24] R. Taniuchi *et al.*, Nature (London) **569**, 53 (2019).
[25] P. Fallon, E. Rodriguez-Vieitez, A. O. Macchiavelli, A. Gade, J. A. Tostevin, Adrich *et al.*, Phys. Rev. C **81**, 041302(R) (2010).
[26] E. O. Cohen, O. Hen, E. Piasetzky, L. B. Weinstein, M. Duer, A. Schmidt *et al.* (CLAS Collaboration), Phys. Rev. Lett. **121**, 092501 (2018).
[27] See the Supplemental Material at http://link.aps.org/supplemental/10.1103/PhysRevLett.125.012501 for (i) the mean beam energies at the entrance of the target, the measured cross sections and the associated statistical and systematic uncertainties, (ii) one-dimensional projections of scattering angles in the plane perpendicular to the beam axis for the reaction channel $^{81}$Ga$(p,3p)$, (iii) a comparison of the angular distributions of $^{81}$Ga$(p,3p)$ for the pair breakup and pair knockout models when using different momentum distributions of the nucleons inside the pair, and (iv) the angular distributions for $^{69}$Co$(p,3p)$ and $^{70}$Ni$(p,3p)$.
[28] A. Obertelli *et al.*, Eur. Phys. J. A **50**, 8 (2014).
[29] M. Hesse *et al.*, Z. Phys. A **355**, 69 (1996).
[30] N. Fukuda, T. Kubo, T. Ohnishi, N. Inabe, H. Takeda, D. Kameda, and H. Suzuki, Nucl. Instrum. Methods Phys. Res., Sect. B **317**, 323 (2013).
[31] P. V. Hough, Method and means for recognizing complex patterns, US Patent No. 3,069,654 (1962).
[32] R. Duda and P. Hart, Commun. ACM **15**, 11 (1972).
[33] C. Santamaria *et al.*, Nucl. Instrum. Methods Phys. Res., Sect. A **905**, 138 (2018).
[34] T. Kubo *et al.*, Prog. Theor. Exp. Phys. **2012**, 03C003 (2012).
[35] N. Paul *et al.*, Phys. Rev. Lett. **122**, 162503 (2019).
[36] C. Santamaria *et al.*, Phys. Rev. Lett. **115**, 192501 (2015).
[37] N. Paul *et al.*, Phys. Rev. Lett. **118**, 032501 (2017).
[38] F. Flavigny *et al.*, Phys. Rev. Lett. **118**, 242501 (2017).
[39] M. Lettmann *et al.*, Phys. Rev. C **96**, 011301 (2017).
[40] S. Chen *et al.*, Phys. Rev. C **95**, 041302 (2017).
[41] L. Olivier *et al.*, Phys. Rev. Lett. **119**, 192501 (2017).
[42] C. Shand *et al.*, Phys. Lett. B **773**, 492 (2017).
[43] O. Tarasov and D. Bazin, Nucl. Instrum. Methods Phys. Res., Sect. B **376**, 185 (2016).
[44] L. Audirac *et al.*, Phys. Rev. C **88**, 041602(R) (2013).
[45] R. Bass, Nucl. Phys. **A231**, 45 (1974).
[46] R. A. Arndt, I. I. Strakovsky, and R. L. Workman, Int. J. Mod. Phys. A **18**, 449 (2003).
[47] C. A. Bertulani and C. De Conti, Phys. Rev. C **81**, 064603 (2010).
[48] C. Colle, W. Cosyn, and J. Ryckebusch, Phys. Rev. C **93**, 034608 (2016).
[49] K. Hatanaka *et al.*, Phys. Rev. C **66**, 044002 (2002).
[50] D. Pérez-Loureiro *et al.*, Phys. Lett. B **703**, 552 (2011).
[51] J. Benlliure *et al.*, Phys. Rev. C **78**, 054605 (2008).
[52] B. Blank *et al.*, Phys. Rev. C **50**, 2398 (1994).
[53] M. Mocko *et al.*, Phys. Rev. C **74**, 054612 (2006).
[54] O. B. Tarasov *et al.*, Phys. Rev. C **87**, 054612 (2013).
[55] T. Enqvist *et al.*, Nucl. Phys. **A686**, 481 (2001).
[56] A. Stolz *et al.*, Phys. Rev. C **65**, 064603 (2002).
[57] J. Cugnon, C. Volant, and S. Vuillier, Nucl. Phys. **A620**, 475 (1997).

[58] J. Allison *et al.*, Nucl. Instrum. Methods Phys. Res., Sect. A **835**, 186 (2016).
[59] We did not include the relative angles $\lambda$ in the fit as they are dependent on the $\theta$ and $\varphi$ angles, and seem to be more sensitive to the limitations of the kinematical models.
[60] M. Vergnes, G. Rotbard, F. Guilbaut, D. Ardouin, C. Lebrun, E. Flynn, D. Hanson, and S. Orbesen, Phys. Lett. **72B**, 447 (1978).
[61] X. Ji, Phys. Rev. Lett. **78**, 610 (1997).
[62] M. Hattawy, N. A. Baltzell, R. Dupré, K. Hafidi, S. Stepanyan, S. Bültmann *et al.* (CLAS Collaboration), Phys. Rev. Lett. **119**, 202004 (2017).
[63] H. Niikura, F. Légaré, R. Hasbani, A. D. Bandrauk, M. Y. Ivanov, D. M. Villeneuve, and P. B. Corkum, Nature (London) **417**, 917 (2002).
[64] P. B. Corkum and F. Krausz, Nat. Phys. **3**, 381 (2007).